

Electromagnetically-induced-absorption-like ground state cooling in a hybrid optomechanical system

Yaoyong Dong(董耀勇), Xuejun Zheng(郑学军), Denglong Wang(王登龙), and Peng Zhao(赵鹏)

Citation: Chin. Phys. B, 2025, 34 (**4**): 044203. DOI: 10.1088/1674-1056/adb260
Journal homepage: http://cpb.iphy.ac.cn; http://iopscience.iop.org/cpb

What follows is a list of articles you may be interested in

Quantum-state engineering using enhanced tripartite interactions in atom-photon-phonon hybrid systems

Yaowu Guo(郭耀武), Jiaqiang Zhao(赵加强), Lianzhen Cao(曹连振), Yingde Li(李英德), and Hong-Yan Lu(路红艳)
Chin. Phys. B, 2025, 34 (**2**): 024203. DOI: 10.1088/1674-1056/ad9a5d

Tunable phonon-atom interaction in a hybrid optomechanical system

Yao Li(李耀), Chuang Li(李闯), Jiandong Zhang(张建东), Ying Dong(董莹), and Huizhu Hu(胡慧珠)
Chin. Phys. B, 2023, 32 (**4**): 044213. DOI: 10.1088/1674-1056/acb9ea

Electromagnetically induced transparency and electromagnetically induced absorption in Y-type system

Kalan Mal, Khairul Islam, Suman Mondal, Dipankar Bhattacharyya, Amitava Bandyopadhyay
Chin. Phys. B, 2020, 29 (**5**): 054211. DOI: 10.1088/1674-1056/ab7ea0

Controllable optical response in hybrid opto-electromechanical systems

Jiang Cheng (江成), Cui Yuan-Shun (崔元顺), Liu Hong-Xiang (刘洪香), Li Xiao-Wei (李晓薇), Chen Gui-Bin (陈贵宾)
Chin. Phys. B, 2015, 24 (**5**): 054206. DOI: 10.1088/1674-1056/24/5/054206

Review of cavity optomechanical cooling

Liu Yong-Chun (刘永椿), Hu Yu-Wen (胡毓文), Wong Chee Wei (黄智维), Xiao Yun-Feng (肖云峰)
Chin. Phys. B, 2013, 22 (**11**): 114213. DOI: 10.1088/1674-1056/22/11/114213

Electromagnetically-induced-absorption-like ground state cooling in a hybrid optomechanical system

Yaoyong Dong(董耀勇)[1], Xuejun Zheng(郑学军)[1,2,†], Denglong Wang(王登龙)[3], and Peng Zhao(赵鹏)[4]

[1] *School of Electromechanical Engineering, Guangdong University of Technology, Guangzhou* 510003, *China*
[2] *School of Mechanical Engineering and Mechanics, Xiangtan University, Xiangtan* 411105, *China*
[3] *School of Physics and Optoelectronics, Xiangtan University, Xiangtan* 411105, *China*
[4] *Science and Technology on Reliability Physics and Application of Electronic Component Laboratory, China Electronic Product Reliability and Environmental Testing Research Institute, Guangzhou* 510610, *China*

(Received 30 October 2024; revised manuscript received 10 January 2025; accepted manuscript online 5 February 2025)

We present a scheme for the electromagnetically-induced-absorption (EIA)-like ground state cooling in a hybrid optomechanical system which is combined by two-level quantum systems (qubits) and a high-Q optomechanical cavity. Under the weak qubit-cavity coupling, the system exhibits an EIA-like effect and this effect is caused by quantum destructive interference that is distinct from the conventional EIA effect driven by quantum constructive interference. More importantly, the EIA-like cooling mechanism can significantly enhance the cooling rate of the hybrid system, enabling the final phonon number beyond the classical cooling limit in the strong optomechanical coupling regime. Meanwhile, the cooling effects of the EIA case is better than that of the normalmode splitting case under the same optomechanical coupling strength and qubit dissipation rate.

Keywords: electromagnetically induced absorption, ground state cooling, optomechanics

PACS: 42.50.–p, 42.50.Gy, 43.58.Wc, 42.50.Lc

DOI: 10.1088/1674-1056/adb260 **CSTR:** 32038.14.CPB.adb260

1. Introduction

Cavity optomechanics have been rapidly developing and attracting a lot of attention,[1,2] since they provide a platform for fundamental studies and applications, including the highly sensitive measurement,[3–5] the quantum information processing,[6–9] observing quantum effects of macroscopic objects,[10,11] and gravitational wave measurement.[12] The ground state cooling of mechanical oscillator, which can reduce harmful thermal noise, is a key technology for realizing the coherence manipulation of mechanical resonators and the optomechanics-based quantum applications.[1,13,14] For this goal, several different ways have been proposed such as cryogenic cooling,[15] feedback cooling,[16–18] and sideband cooling.[19,20] Sideband cooling based on resonantly enhanced anti-Stokes cooling is a classical and widely studied cooling method that has achieved great success in both theory[19,20] and experiment.[21–23] However, there are two main limits in the sideband cooling: the quantum cooling limit caused by quantum backaction and the classical cooling limit caused by environmental thermal noise.

High-Q cavities have extremely low dissipation rates κ, resulting in long photon lifetimes within the cavity and significantly enhanced interactions between photons and matter.[24,25] These characteristics make high-Q cavities exceptionally promising for applications in quantum storage and quantum information processing.[26–28] In high-Q optomechanical cavities, the quantum cooling limit induced by the quantum backaction is very small due to the low dissipation rate κ, and the classical cooling limit becomes the main limiting factor for the ground state cooling. Additionally, due to the influence of normal-mode splitting (NMS),[29] the classical cooling limit becomes $\gamma_{\rm m} n_{\rm th}/\kappa$ in the strong optomechanical coupling regime.[1,13,30,31] At that time, the classical cooling limit is inversely proportional with the cavity dissipation rate, and the pre cooling temperature is constrained by the cavity dissipation rate. On the other hand, by introducing two-level atoms,[32–34] three-level atoms,[35] or auxiliary cavities,[36–38] it is possible to achieve the phenomenon of electromagnetically induced transparency (EIT) in the ground state cooling process. This can realize the suppression of the heating process via the quantum interference effect, thereby potentially achieving the ground state cooling in the unresolved sideband. However, besides the EIT effect,[39] there are also phenomena such as electromagnetically induced absorption (EIA)[40–42] and electromagnetically induced amplification (EIAM)[43] caused by quantum interferences in cold atomic systems.

Inspired by those works, we propose a scheme where the ground state cooling beyond the classical cooling limit can be achieved with EIA-like and NMS effects in a hybrid optomechanical system consisting of an optomechanical cavity and

†Corresponding author. E-mail: zhengxuejun@xtu.edu.cn

© 2025 Chinese Physical Society and IOP Publishing Ltd. All rights, including for text and data mining, AI training, and similar technologies, are reserved.

two-level quantum systems (qubits). In the weak qubit–cavity coupling regime, an EIA-like noise spectrum induced by the quantum destructive interference can be occurred, and meanwhile the final phonon number of the hybrid system can surpass the classical cooling limit of the standard resolved sideband cooling in the strong optomechanical coupling regime due to the EIA-like effect. In the strong qubit–cavity coupling regime, the system exhibits NMS and forms two new splitting modes. Based on the couple of the new modes and the mechanical mode, the system can also achieve the ground state cooling in the strong optomechanical coupling regime. In Section 2, we introduce the hybrid optomechanical system model and discuss its stability. In Section 3, we derive the cooling and heating rates and prove that the ground state cooling of the hybrid system with EIA-like and NMS effects can be achieved in the strong optomechanical coupling regime. Finally, we make a summary of our work and present an outlook in Section 4.

2. Theoretical model

As shown in Fig. 1, the hybrid optomechanical system is composed of two-level quantum systems (qubits) and an optomechanical cavity.

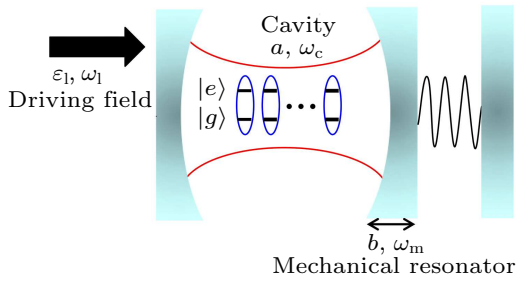


Fig. 1. Schematic diagram of a hybrid cavity optomechanical system where the qubits are placed at an optomechanical cavity with a strong driven field.

The mechanical resonator with frequency ω_m couples to the cavity field via radiation pressure. The mode of the cavity field with frequency ω_c is driven by a pump laser with amplitude ε_l and frequency ω_l. The interaction Hamilton of the qubits and cavity field is given by $H_{int}=\sum_{i=1}^{N_0}\tilde{g}_i(a^\dagger\sigma_i^- + a\sigma_i^+)$ with $\hbar=1$, where $\sigma_i^- = |g_i\rangle\langle e_i|$ and $\sigma_i^+ = |e_i\rangle\langle g_i|$ are the down and rising operators of the i-th qubit, respectively. N_0 is the number of qubits. $|g_i\rangle$, $|e_i\rangle$, and $\tilde{g}_i$ are the ground-state, excite-state, and single-photon coupling strength of the i-th qubit, respectively. a and $a^\dagger$ are annihilation and creation operators of the cavity mode, respectively. The frequency of transition $|g\rangle \leftrightarrow |e\rangle$ is ω_1. Introducing the collective operators $\sigma^- = \sum_{i=1}^{N_0}\sigma_i^-$ and $\sigma^+ = \sum_{i=1}^{N_0}\sigma_i^+$, we use the Holstein–Primakoff transformation,[44–46] and then the collective operators can be written as $\sigma^+ = c^\dagger\sqrt{N_0 - c^\dagger c} \simeq \sqrt{N_0}c^\dagger$ and $\sigma^- = c\sqrt{N_0 - c^\dagger c} \simeq \sqrt{N_0}c$, where c and $c^\dagger$ obey the standard commutator $[c, c^\dagger] \simeq 1$ with N_0 far larger than the number of excited qubits. Based on this, the total Hamilton of the system is ($\hbar=1$)

$$\begin{aligned} H =\ & \omega_c a^\dagger a + \omega_m b^\dagger b + \omega_l c^\dagger c + g a^\dagger a(b^\dagger + b) \\ & + g_1(a^\dagger c + a c^\dagger) + i\varepsilon_l(a^\dagger e^{-i\omega_l t} - a e^{i\omega_l t}), \end{aligned} \tag{1}$$

where $g_1 = \sqrt{N_0}\bar{g}_0$ is the collective qubit–photon coupling strength with $\bar{g}_0 = \sum_{i=1}^{N_0}\tilde{g}_0^{(i)}/N_0$. The first, second, and third terms denote the free Hamilton of the cavity, mechanical resonator, and qubits, respectively. The fourth (fifth) term denotes the interaction Hamilton between the cavity mode and mechanical resonator (qubits) with the coupling strength g (g_1). The last term represents the Hamilton of the driving field coupled to the cavity mode. b and $b^\dagger$ are annihilation and creation operators of the mechanical mode, respectively. The annihilation and creation operators satisfy the commutation relations $[n, n^\dagger]=1$ with $n=a, b$. Using a unitary transformation $\tilde{H} = UHU^\dagger - iU\partial U^\dagger/\partial t$ with $U = \exp\left[i\omega_l a^\dagger a t + i\omega_l c^\dagger c t\right]$,[1] the Hamilton in the rotating frame is

$$\begin{aligned} H =\ & \Delta a^\dagger a + \omega_m b^\dagger b + \Delta_c c^\dagger c + g a^\dagger a(b^\dagger + b) \\ & + g_1(a^\dagger c + a c^\dagger) + i\varepsilon_l(a^\dagger - a), \end{aligned} \tag{2}$$

where $\Delta = \omega_c - \omega_l$, $\Delta_c = \omega_l - \omega_l$, and $\Delta_p = \omega_p - \omega_l$. Using the Hamilton (2), the Heisenberg–Langevin equations can be obtained as

$$\begin{aligned} \dot{b} &= -\left(i\omega_m + \frac{\gamma_m}{2}\right)b - iga^\dagger a + \sqrt{\gamma_m}b_{in}, \\ \dot{a} &= -\left(i\Delta + \frac{\kappa}{2}\right)a - iga(b^\dagger + b) - ig_1 c + \varepsilon_l + \sqrt{\kappa}a_{in}. \end{aligned} \tag{3}$$

Here γ, γ_m, and κ denote the dissipation rates of the qubits, mechanical resonator, and cavity mode, respectively. f_{in}, b_{in}, and a_{in} represent the corresponding noise operators with zero mean values. The correlation functions for these noise operators are given by $\langle f_{in}^\dagger(t) f_{in}(t')\rangle = 0$, $\langle f_{in}(t) f_{in}^\dagger(t')\rangle = \delta(t-t')$, $\langle b_{in}^\dagger(t) b_{in}(t')\rangle = n_{th}\delta(t-t')$, $\langle b_{in}(t) b_{in}^\dagger(t')\rangle = (n_{th}+1)\delta(t-t')$, $\langle a_{in}^\dagger(t) a_{in}(t')\rangle = 0$, and $\langle a_{in}(t) a_{in}^\dagger(t')\rangle = \delta(t-t')$.[32,47,48] The environmental thermal phonon number n_{th} of the mechanical resonator is expressed as $n_{th} = [\exp(\hbar\omega_m/k_B T) - 1]^{-1}$ where k_B and T are the Boltzmann constant and environmental temperature, respectively. We adopt the usual linearized approach and then the operators in Eq. (3) can be rewrite as the sum of the steady-state values and the small fluctuations, i.e., $a = \alpha + \delta a$, $c = C_0 + \delta c$, $b = \beta + \delta b$. With the means field approximation $\langle AB\rangle = \langle A\rangle\langle B\rangle$,[49,50] the mean values are given by

$$\begin{aligned} \beta &= -\frac{ig|\alpha|^2}{(i\omega_m + \gamma_m/2)}, \quad C_0 = -\frac{ig_1\alpha}{(i\Delta_c + \gamma/2)}, \\ \alpha &= \frac{\varepsilon_l}{i\Delta' + \kappa/2 + g_1^2/(i\Delta_c + \gamma/2)}, \end{aligned} \tag{4}$$

where $\Delta' = \Delta + 2g\,\mathrm{Re}[\beta]$ is the modified detuning. After that, the effective linearized Hamilton is given by the following expression

$$H_{\rm lin} = \Delta'\delta a^\dagger \delta a + \omega_{\rm m}\delta b^\dagger \delta b + \Delta_{\rm c}\delta c^\dagger \delta c + G(\delta a^\dagger + \delta a)(\delta b^\dagger + \delta b) + g_1(\delta a^\dagger \delta c + \delta a \delta c^\dagger), \quad (5)$$

where $G = g\sqrt{\bar{n}_{\rm cav}}$ is the optomechanical coupling strength which is enhanced by the cavity field with the mean photon number $\bar{n}_{\rm cav} = |\alpha|^2$. Note that, the influence of the higher order small term $\delta a^\dagger \delta a$ has been ignored. The linearized Heisenberg–Langevin equations based on the effective linearized Hamilton (5) are given by

$$\begin{aligned}
\delta\dot{c} &= -\left(\mathrm{i}\Delta_{\rm c} + \frac{\gamma}{2}\right)\delta c - \mathrm{i}g_1\delta a + \sqrt{\gamma}f_{\rm in},\\
\delta\dot{b} &= -\left(\mathrm{i}\omega_{\rm m} + \frac{\gamma_{\rm m}}{2}\right)\delta b - \mathrm{i}G(\delta a^\dagger + \delta a) + \sqrt{\gamma_{\rm m}}b_{\rm in},\\
\delta\dot{a} &= -\left(\mathrm{i}\Delta' + \frac{\kappa}{2}\right)\delta a - \mathrm{i}G(\delta b^\dagger + \delta b) - \mathrm{i}g_1\delta c + \sqrt{\kappa}a_{\rm in}. \quad (6)
\end{aligned}$$

Until now, we have established the Hamiltonian of the hybrid optomechanical system and derived the linearized Heisenberg–Langevin equations for the operators. Then, the stability of the system is discussed in here, and we thus introduce the quadrature operators $X_n = (n^\dagger + n)/2$ and $Y_n = (n - n^\dagger)/(2\mathrm{i})$ with $n = [\delta a, \delta b, \delta c]$. The motion equation for the quadrature operators is

$$\dot{R}(t) = AR(t) + N(t), \quad (7)$$

where the coefficient matrix is

$$A = \begin{pmatrix}
-\gamma/2 & \Delta_{\rm c} & 0 & g_1 & 0 & 0\\
-\Delta_{\rm c} & -\gamma/2 & -g_1 & 0 & 0 & 0\\
0 & g_1 & -\kappa/2 & \Delta' & 0 & 0\\
-g_1 & 0 & -\Delta' & -\kappa/2 & -2G & 0\\
0 & 0 & 0 & 0 & -\gamma_{\rm m}/2 & \omega_{\rm m}\\
0 & 0 & -2G & 0 & -\omega_{\rm m} & -\gamma_{\rm m}/2
\end{pmatrix}. \quad (8)$$

Here $R(t) = [X_{\rm c}(t),\ Y_{\rm c}(t),\ X_{\rm a}(t),\ Y_{\rm a}(t),\ X_{\rm b}(t),\ Y_{\rm b}(t)]^{\rm T}$ is the vector of the quadrature operators for the cavity field, mechanical resonator, and qubits, and $N(t) = [X^{\rm c}_{\rm in}(t), Y^{\rm c}_{\rm in}(t), X^{\rm a}_{\rm in}(t), Y^{\rm a}_{\rm in}(t), X^{\rm b}_{\rm in}(t), Y^{\rm b}_{\rm in}(t)]^{\rm T}$ is the vector of the corresponding noise quadrature operators with $X_{\rm in} = (n^\dagger_{\rm in} + n_{\rm in})/2$, $Y_{\rm in} = (n_{\rm in} - n^\dagger_{\rm in})/(2\mathrm{i})$, and $n_{\rm in} = [a_{\rm in}, b_{\rm in}, f_{\rm in}]$. The system dynamics is stable if and only if all of the eigenvalues of Ahave negative real parts.

Figure 2 shows the steady range of the system for different conditions. As shown in Figs. 2(a) and 2(b), when the qubit–cavity coupling strength is small ($g_1 = 0.25\omega_{\rm m}$), the system can achieve stability in the red detuning regime, while when the qubit–cavity coupling strength is large ($g_1 = 2\omega_{\rm m}$), the system can form the NMS, and the system can achieve stability in the blue detuning regime and the detuning Δ_1 ($\Delta_1 = \Delta' = \Delta_{\rm c}$) greater than $1.7\omega_{\rm m}$. In addition, combining Figs. 2(a) and 2(b), it can be seen that the system cannot be in the dissipative–active case, but have a good stability in the dissipative–dissipative case, that is, the ranges of used stable parameters are wide in the dissipative–dissipative case.

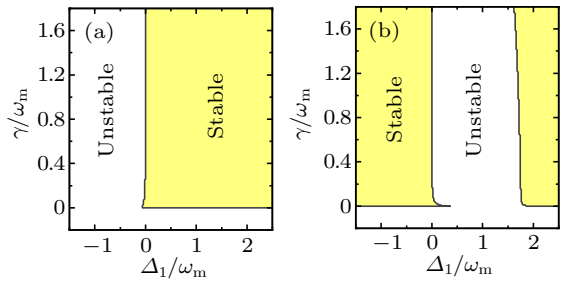


Fig. 2. The stable boundary of the system for difference parameters: (a) $g_1 = 0.25\omega_{\rm m}$ and (b) $g_1 = 2\omega_{\rm m}$, with $G = 0.05\omega_{\rm m}$ and $\kappa = 0.01\omega_{\rm m}$. Here we set $\Delta_1 = \Delta' = \Delta_{\rm c}$ and take $\gamma_{\rm m} = 10^{-5}\omega_{\rm m}$.

3. Cooling dynamics and results

In this section, we will give the cooling and heating rates and the final phonon number through the quantum noise approach.[13] Meanwhile, we also give the numerical result of the phonon number by using the covariance matrix approach[13] for comparing with that obtained by the noise spectrum approach.

3.1. Cooling rate

When the qubit–cavity coupling is far stronger than the optomechanical coupling, i.e., $g_1 \gg G$, we consider the coupling of the optical field and the qubits to form new modes, and a mechanical resonator coupling with the new modes through optomechanical interactions. Therefore, we assume that the qubit–cavity coupling subsystem as the environmental bath for the mechanical resonator and the optomechanical interaction as a perturbation to this environmental bath. Using the noise spectrum approach, the cooling and heating rates can be given by

$$A_\pm = G^2 S(\mp\omega_{\rm m}), \quad (9)$$

where

$$S(\omega) = \int_{-\infty}^{\infty} \langle F(\tau)F(0)]\rangle\, \mathrm{e}^{\mathrm{i}\omega\tau}\,\mathrm{d}\tau \quad (10)$$

is the noise spectrum of the optical force $F = \delta a^\dagger + \delta a$.[34,36] To obtain the expression of $S(\omega)$, we can solve the linearized Heisenberg–Langevin equations (6) in the frequency domain, and the expression of $\delta a(\omega)$ can be given as

$$\delta a(\omega) = \frac{1}{\mathrm{i}(\Delta' - \omega) + \frac{\kappa}{2} + \frac{g_1^2}{\mathrm{i}(\Delta_{\rm c} - \omega) + \gamma/2}} \times \left[\sqrt{\kappa}a_{\rm in}(\omega) + \frac{-\mathrm{i}g_1\sqrt{\gamma}f_{\rm in}(\omega)}{\mathrm{i}(\Delta_{\rm c} - \omega) + \gamma/2}\right] \quad (11)$$

with the perturbation approximation. Thus, the noise spectrum $S(\omega)$ is given by

$$S(\omega) = \frac{1}{|L(\omega)|^2}\left[\kappa + \frac{g_1^2\gamma}{|\mathrm{i}(\Delta_c-\omega)+\gamma/2|^2}\right] = \left[\frac{1}{L(\omega)}+\frac{1}{L^*(\omega)}\right]\left\{\frac{\kappa+\dfrac{g_1^2\gamma}{(\Delta_c-\omega)^2+\gamma^2/4}}{2\mathrm{Re}\,[L(\omega)]}\right\}, \quad (12)$$

where

$$L(\omega) = \mathrm{i}(\Delta'-\omega)+\frac{\kappa}{2}+\frac{g_1^2}{\mathrm{i}(\Delta_c-\omega)+\gamma/2}. \quad (13)$$

Then, $2\mathrm{Re}[L(\omega)]$ can be written as $\kappa + g_1^2\gamma/[(\Delta_c-\omega)^2+\gamma^2/4]$. Therefore, the noise spectrum $S(\omega)$ can be rewritten as

$$S(\omega) = \frac{1}{L(\omega)}+\frac{1}{L^*(\omega)}. \quad (14)$$

According to the dressed-states theory,[51] the expression (14) can be rewritten as

$$S(\omega) = S_+(\omega)+S_-(\omega) \quad (15)$$

with

$$S_+(\omega) = \frac{B_+}{\mathrm{i}(\Delta_1-\omega-x_+)}+\frac{B_+^*}{-\mathrm{i}(\Delta_1-\omega-x_+^*)}, \quad (16)$$

$$S_-(\omega) = \frac{B_-}{\mathrm{i}(\Delta_1-\omega-x_-)}+\frac{B_-^*}{-\mathrm{i}(\Delta_1-\omega-x_-^*)}, \quad (17)$$

where $x_\pm = \mathrm{i}(\gamma+\kappa)/4 \pm X/4$, $B_\pm = \pm(x_\pm - \mathrm{i}\gamma/2)/(x_+-x_-)$, and $X = \sqrt{16g_1^2-(\kappa+\gamma)^2}$. Here the complex number $\Delta_1 - x_\pm$ corresponds to two new modes $\omega_\pm = \Delta_1 - \mathrm{Re}\,x_\pm$. In the weak qubit–cavity coupling regime ($g_1 < (\kappa+r)/4$), the two modes $\omega_\pm$ are degenerate, and therefore various quantum interferences can be generated between the two-mode transition paths.[52] In the strong qubit–cavity coupling regime ($g_1 \gg (\kappa+\gamma)/4$), the two modes $\omega_\pm$ are splitting into $\omega_\pm \approx \Delta_1 \pm g_1$, which means the formation of NMS in the hybrid system. The corresponding operators for two new modes $\omega_\pm = \Delta_1 - \mathrm{Re}\,x_\pm$ can be expressed by c_+ and c_- with $\delta a^\dagger = h_{21}c_+^\dagger + h_{31}c_-^\dagger$, $\delta a = h_{12}c_+ + h_{13}c_-$, $\delta c = -g_1(h_{12}x_-c_+ + h_{13}x_+c_-)/x_+x_-$, and $\delta c^\dagger = -(h_{21}x_-c_+^\dagger + h_{31}x_+c_-^\dagger)/g_1$. Here, the coefficients are given by

$$h_{12} = -(x_- - \mathrm{i}\gamma/2)/\sqrt{g_1^2+(x_- - \mathrm{i}\gamma/2)^2},$$
$$h_{13} = -(x_+ - \mathrm{i}\gamma/2)^2\sqrt{g_1^2+(x_+ - \mathrm{i}\gamma/2)^2},$$
$$h_{21} = \sqrt{g_1^2+(x_- - \mathrm{i}\gamma/2)^2}/(x_+-x_-),$$
$$h_{31} = -\sqrt{g_1^2+(x_+ - \mathrm{i}\kappa/2)^2}/(x_+-x_-).$$

The coefficient $h_{12(13)}$ represents the coupling factors between the corresponding modes and mechanical resonator, and there are $B_+ = h_{12}h_{21}$ and $B_- = h_{13}h_{31}$. According to the dressed-states theory, we can analyze the quantum interference and NMS effects in this hybrid system through the noise spectra $S_\pm(\omega)$ of the modes $\omega_\pm$.

In $g_1 < (\kappa+\gamma)/4$ regime, the corresponding modes $\omega_\pm$ are degenerate where X is a pure imaginary number, and they could from various quantum interference effects. According to Ref. [52], the dipole correlation between the effective dipole moments $\boldsymbol{\mu}_+$ and $\boldsymbol{\mu}_-$ of the two modes can be represented as $p = \boldsymbol{\mu}_+\cdot\boldsymbol{\mu}_-/|\boldsymbol{\mu}_+||\boldsymbol{\mu}_-|$ $(-1<p<1)$, which will result in the quantum interference phenomena. The dissipation rates κ and γ as well as the parameter p satisfy $\kappa-\gamma = p(\kappa+\gamma)$,[52] and thus we have $p = (\kappa-\gamma)/(\kappa+\gamma)$. We plot the noise spectrum $S(x)$ as a function of x with different parameters p. From Fig. 3, we clearly see that the hybrid system displays an EIT-like line shape at $p>0$ and an EIA-like line shape at $p<0$ which is similar to the EIT and EIA phenomena in the three-level resonators system.[52,53]

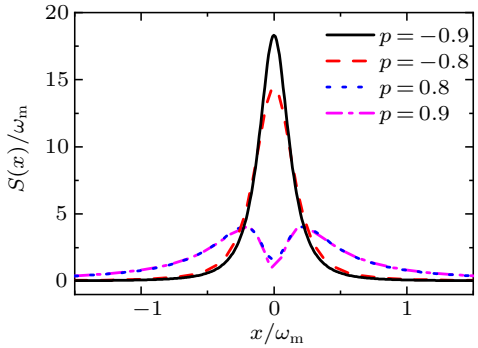


Fig. 3. Noise spectrum $S(x)$ as a function of $x=\omega-\omega_m$ for $p=-0.9$, -0.8, 0.8, 0.9 when $g_1=0.2\omega_m$ and $\Delta_1=\omega_m$. Here the parameters $p=-0.9$, -0.8, 0.8, 0.9 correspond to $\gamma=0.95\omega_m$, $0.85\omega_m$, $0.15\omega_m$, $0.05\omega_m$ and $\kappa=0.05\omega_m$, $0.15\omega_m$, $0.85\omega_m$, $0.95\omega_m$.

For further studying the EIT- and EIA-like effects, we plot the noise spectra $S(x)$, $S_+(x)$, and $S_-(x)$ as a function of x in the EIT and EIA cases in Fig. 4. Moreover, the quantum interference is maximal at the two-photon resonance point no matter at $p>0$ or $p<0$. In the EIT case, the noise spectrum $S_-(x)$ is positive and the noise spectrum $S_+(x)$ is negative, and they both appear medium-sized peaks, as shown in Fig. 4(a). This means that the quantum destructive interference is formed between the transition paths between the two modes and the mechanical resonator, resulting in the EIT-like effect. For $p<0$, it can be found that the EIA-like effect is also origin to the quantum destructive interference. However, the noise spectrum $S_-(x)$ is negative with a small peak while the noise spectrum $S_+(x)$ is positive with a large peak in the EIA case as shown in Fig. 4(b), which denotes the quantum destructive interference is contrary to the EIT case. Therefore, this EIA-like effect in the hybrid optomechanical system is different to the EIA effect caused by the quantum constructive interference in four-level atomic systems.[38,39] The EIT and EIA cases, causing by the quantum interference, both require

a weak qubit–cavity coupling strength, i.e., $g_1 < (\kappa+\gamma)/4$. However, the EIT case needs $\kappa > \gamma$, while the EIA case needs $\gamma > \kappa$. Additionally, there is a dip at the two-photon resonance point in the noise spectrum with the EIT case, whereas there is a large peak under the EIA case. Therefore, the EIA-like effect can induce larger cooling rate than the EIT-like effect for resolved sideband systems with a small κ at the two-photon resonance point of the noise spectrum.

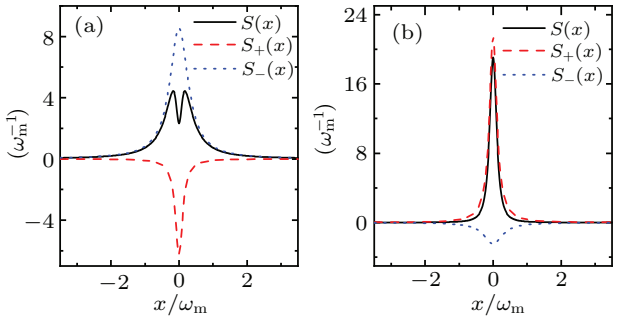


Fig. 4. Noise spectra $S(x)$, $S_+(x)$, and $S_-(x)$ as a function of x in (a) the EIT case $p > 0$ with $\kappa = 0.82\omega_m$ and $\gamma = 0.1\omega_m$, and (b) the EIA case $p < 0$ with $\kappa = 0.1\omega_m$ and $\gamma = 0.82\omega_m$. The qubit–cavity coupling strength takes $g_1 = 0.15\omega_m$ and the detuning is $\Delta_1 = \omega_m$.

According to Eq. (9), the cooling and heating rates can be rewritten as $A_\pm = G^2\,\mathrm{Re}[S(\Delta_1 \pm \omega_m)]$, and the net optical damping rate is $\Gamma_{opt} = A_- - A_+$.[1,13] Therefore, in the EIA case, the maximal cooling rate is corresponding to the peak of EIA-like line shape, namely, $A_- = G^2\,\mathrm{Re}\,S(0)$ with $\Delta_1 = \omega_m$. When $4g_1^2 \gg \gamma\kappa$, its expression can be written as

$$A_- \approx \frac{\gamma G^2}{g_1^2}. \tag{18}$$

At this condition, the corresponding heating rate is $A_+ = G^2 S(2\omega_m)$, and its expression is

$$A_+ \approx \frac{G^2 g_1^2 \gamma}{16\omega_m^4 + \gamma^2\omega_m^2}. \tag{19}$$

When $g_1 \gg (\kappa+\gamma)/4$, the system is in the NMS regime with the corresponding modes splitting into $\omega_\pm \approx \Delta_1 \pm g_1$. Here, we plot the noise spectra $S(x)$, $S_+(x)$, and $S_-(x)$ as a function of x for the NMS case in Fig. 5. From Fig. 5, it can be seen that the quantum interference of the system is very small no matter with $p > 0$ or $p < 0$ in the NMS regime. Meanwhile, there are two splitting peaks at $x = \pm g_1$ both of $p > 0$ and $p < 0$, indicating that the NMS cooling mechanism does not require to satisfy $\gamma > \kappa$ or $\gamma < \kappa$. The optimal cooling rate is obtained by taking $\Delta_1 = \pm X + \omega_m$ according to Eqs. (16) and (17), and it can be written as $\Delta_1 \approx \pm g_1 + \omega_m$ when $g_1 \gg \gamma$, κ. As shown in Fig. 5, the cooling rate $A_- = G^2 S(-g_1)$ with $\Delta_1 \approx -g_1 + \omega_m$ are corresponding to one of the resonance peaks in the noise spectrum. The corresponding heating rate is $A_+ = G^2 S(-g_1 + 2\omega_m)$ which is corresponding to the NMS dip. The expressions of A_- and A_+ are given by

$$A_- \approx \frac{4G^2}{\gamma}, \tag{20}$$

$$A_+ \approx \frac{4G^2 g_1^2 \gamma}{\gamma^2(2\omega_m - g_1)^2 + 64(\omega_m - g_1)^2\omega_m^2} \tag{21}$$

with $4g_1^2 \gg \gamma\kappa$ and $\gamma \gg \kappa$. Furthermore, the net cooling rate Γ_{opt} as functions of g_1 and Δ_1 is shown in Fig. 6. It clearly sees that the system is becoming from the EIA case to the NMS case with increasing g_1. The negative value of Γ_{opt} denotes the heating effect, and the positive value of Γ_{opt} denotes the cooling effect. In the NMS regime, the net cooling rate Γ_{opt} has a large value near two splitting peak points, which means the optimal cooling condition is $\Delta_1 \approx \pm g_1 + \omega_m$, as shown in Fig. 6. In the EIA regime, there is a maximal net cooling rate at the EIA-like induced peak, and this maximal net cooling rate is larger than that in the NMS regime. In other word, the cooling effect of the hybrid system can be improved by adopted the EIA cooling scheme with the same qubit dissipation rate. The blue negative range is the peak range of the net heating process. When $g_1 = \omega_m$ and $\Delta_1 - \omega_m = 0$, the cooling and heating processes are both in resonance and thus the net cooling rate is vanished.

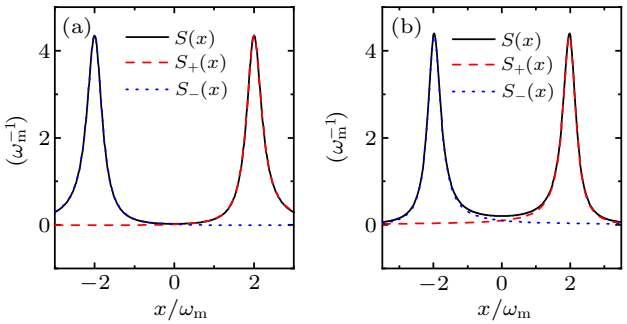


Fig. 5. Noise spectra $S(x)$, $S_+(x)$, and $S_-(x)$ as a function of x in the NMS case at (a) $p > 0$ with $\kappa = 0.82\omega_m$ and $\gamma = 0.1\omega_m$, (b) $p < 0$ with $\kappa = 0.1\omega_m$ and $\gamma = 0.82\omega_m$. The qubit–cavity coupling strength takes $g_1 = 2\omega_m$ and the detuning is $\Delta_1 = \omega_m$.

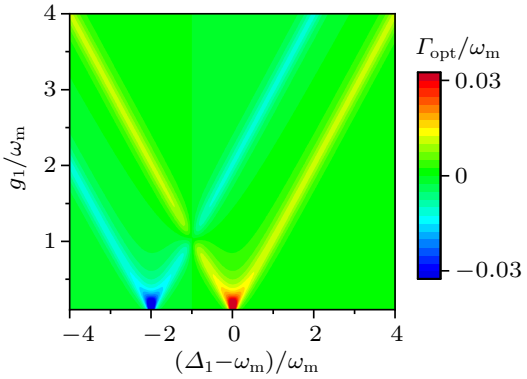


Fig. 6. The net cooling rate Γ_{opt} versus the coupling strength g_1 and the detuning Δ_1 with the parameters: $G = 0.05\omega_m$, $\kappa = 0.01\omega_m$, and $\gamma = 0.85\omega_m$.

3.2. Phonon number

The average phonon number $\bar{n}$ is given as

$$\bar{n} = \sum_{n=0}^{\infty} nP_n.$$

Here $P_n = \langle n|\rho_{\rm b}|n\rangle$ is the probability of the Fock state $|n\rangle$ and satisfies the following equation:

$$\begin{aligned}\dot{P}_n =& [\gamma_{\rm m}(n_{\rm th}+1)+A_-][(n+1)P_{n+1}-nP_n]\\ &+(\gamma_{\rm m}n_{\rm th}+A_+)(nP_{n-1}-nP_n).\end{aligned} \tag{22}$$

Combing the Eq. (22), we can obtain the motion equation of average phonon number as

$$\dot{\bar{n}} = (\bar{n}+1)(A_+ + \gamma_{\rm m}n_{\rm th}) - \bar{n}[A_- + \gamma_{\rm m}(n_{\rm th}+1)]. \tag{23}$$

According to Eq. (23), the final phonon number $n_{\rm f}$ is given as

$$n_{\rm f} = \frac{A_+ + n_{\rm th}\gamma_{\rm m}}{\Gamma_{\rm opt}+\gamma_{\rm m}} \tag{24}$$

with the steady-state condition, i.e., $\dot{\bar{n}} = 0$. In the above expression (24) $A_+/(\Gamma_{\rm opt}+\gamma_{\rm m})$ and $n_{\rm th}\gamma_{\rm m}/(\Gamma_{\rm opt}+\gamma_{\rm m})$ are induced by the quantum backaction and the thermal noise, respectively. Therefore, in the EIA case, the final phonon numbers induced by the thermal noise and the quantum backaction are

$$n_1^{\rm EIA} \approx \frac{\gamma_{\rm m}g_1^2 n_{\rm th}}{G^2\gamma}, \tag{25}$$

$$n_2^{\rm EIA} \approx \frac{g_1^4}{16\omega_{\rm m}^4+\gamma^2\omega_{\rm m}^2}. \tag{26}$$

The final phonon numbers in the NMS case due to the thermal noise and the quantum backaction are given by

$$n_1^{\rm NMS} \approx \frac{\gamma_{\rm m}n_{\rm th}\gamma}{4G^2}, \tag{27}$$

$$n_2^{\rm NMS} \approx \frac{g_1^2\gamma^2}{\gamma^2(2\omega_{\rm m}-g_1)^2+64(\omega_{\rm m}-g_1)^2\omega_{\rm m}^2}. \tag{28}$$

For the exact solution of the final phonon number, we give the master equation

$$\begin{aligned}\dot{\rho} =& \,{\rm i}[\rho,H]+\frac{\gamma}{2}(2\delta c\rho\delta c^\dagger-\delta c^\dagger\delta c\rho-\rho\delta c^\dagger\delta c)\\ &+\frac{\kappa}{2}(2\delta a\rho\delta a^\dagger-\delta a^\dagger\delta a\rho-\rho\delta a^\dagger\delta a)\\ &+\frac{\gamma_{\rm m}}{2}(n_{\rm th}+1)(2\delta b\rho\delta b^\dagger-\delta b^\dagger\delta b\rho-\rho\delta b^\dagger\delta b)\\ &+\frac{\gamma_{\rm m}}{2}n_{\rm th}(2\delta b^\dagger\rho\delta b-\delta b\delta b^\dagger\rho-\rho\delta b\delta b^\dagger).\end{aligned} \tag{29}$$

The average phonon number $\langle\delta b^\dagger\delta b\rangle$ can be calculated by ${\rm Tr}(\rho\delta b^\dagger\delta b)$.

Then, we plot the phonon number under the steady-state condition as a function of G for the EIA case with different coupling strengths g_1 and the NMS case with different dissipations γ in Figs. 7(a) and 7(b), respectively. Note that, the analytical results are given by Eq. (24) and the numerical results are based on Eq. (28). From Fig. 7, we see that the analytical solution is agree with the numerical solution when G is smaller than g_1. When G approaches g_1, the deviation between the analytical and numerical solutions also becomes larger, because our analytical results are solved by the perturbation approximation under $G \ll g_1$. This is due to the hybridization of the oscillator's motion with the optical field and the qubits,[29] so that the optomechanical coupling cannot be treated as a perturbation when its strength approaches to the qubit–cavity coupling strength.

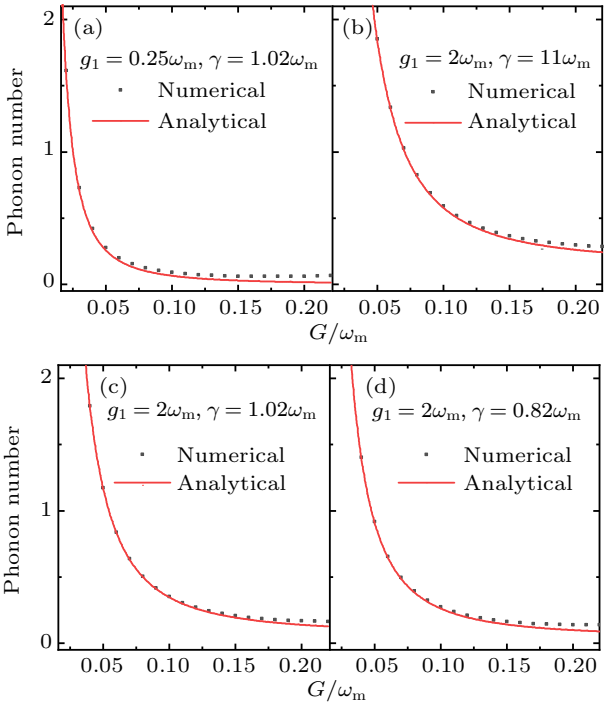


Fig. 7. Phonon number as a function of G in the EIA case with $\Delta_1 = \omega_{\rm m}$ for (a) $g_1 = 0.25\omega_{\rm m}$ and $\gamma = 1.02\omega_{\rm m}$; (b) $g_1 = 2\omega_{\rm m}$ and $\gamma = 11\omega_{\rm m}$. The final phonon number as a function of G in NMS case with $\Delta_1 = -\omega_{\rm m}$ for (c) $\gamma = 1.02\omega_{\rm m}$ and (d) $\gamma = 0.82\omega_{\rm m}$ with $g_1 = 2\omega_{\rm m}$. Both of two cases take $\kappa = 0.01\omega_{\rm m}$, $\gamma_{\rm m} = 10^{-5}\omega_{\rm m}$, and $n_{\rm th} = 1000$.

As seem from Figs. 4 and 5, we have known that the cooling rate is far garter than the heating rate in the EIA and NMS cases, i.e., $A_- \gg A_+$. At that time, we consider that the final phonon number is mainly dependent on the thermal noise. Thus, the final phonon number can approximately rewrite as $n_{\rm f} \approx n_{\rm th}\gamma_{\rm m}/A_-$. We have $n_{\rm f-EIA} = \gamma_{\rm m}g_1^2 n_{\rm th}/G^2\gamma$ and $n_{\rm f-NMS} = \gamma_{\rm m}n_{\rm th}\gamma/4G^2$ in the EIA and NMS cases, respectively. For realizing $n_{\rm f} < 1$, it is needed that the optomechanical coupling strength satisfies $G_{\rm EIA} > g_1\sqrt{\gamma_{\rm m}n_{\rm th}/\gamma}$ and $G_{\rm NMS} > \sqrt{\gamma_{\rm m}n_{\rm th}\gamma}/2$ in the EIA and NMS cases, respectively. For the EIA case, the mechanical resonator can be cooled to its ground state with a smaller G when $g_1/\sqrt{\gamma}$ is smaller, while a larger G is required for cooling the mechanical resonator to its ground state when $g_1/\sqrt{\gamma}$ is larger, as shown in

Figs. 7(a) and 7(b). In the NMS case, the mechanical resonator cooling to its ground state requires a smaller G when γ is smaller, and the reverse applies when γ is larger, as shown in Figs. 7(c) and (d). When the ground state cooling in the system goes beyond the classical cooling limit, the final phonon numbers for the EIA and NMS cooling mechanisms must respectively satisfy $n_{\mathrm{f-EIA}} < \gamma_{\mathrm{m}} n_{\mathrm{th}}/\kappa$ and $n_{\mathrm{f-NMS}} < \gamma_{\mathrm{m}} n_{\mathrm{th}}/\kappa$, where $\gamma_{\mathrm{m}} n_{\mathrm{th}}/\kappa$ represents the classical cooling limit.[1,13,30,31] At that time, the corresponding optomechanical coupling strengths under the EIA and NMS cases must satisfy $G > g_1\sqrt{\kappa/\gamma}$ and $G > \sqrt{\kappa/\gamma}/2$, respectively. For $\gamma_{\mathrm{m}} n_{\mathrm{th}} < \kappa$, the classical sideband cooling mechanism is unable to cooling the mechanical resonator to it ground state, while the ground state cooling can be achieved with the EIA cooling mechanism and the classical cooling limit can be surpassed when $G > g_1\sqrt{\gamma_{\mathrm{m}} n_{\mathrm{th}}/\gamma}$ is satisfied. For $\gamma_{\mathrm{m}} n_{\mathrm{th}} < \kappa$, the EIA cooling mechanism can achieve the ground state cooling but cannot realize to beyond the classical cooling limit within the range of $g_1\sqrt{\kappa/\gamma} > G > g_1\sqrt{\gamma_{\mathrm{m}} n_{\mathrm{th}}/\gamma}$. Similarly, the ground state cooling beyond the classical cooling limit can also be achieved in the NMS case when $\gamma_{\mathrm{m}} n_{\mathrm{th}} > \kappa$ and $G > \sqrt{\gamma_{\mathrm{m}} n_{\mathrm{th}}\gamma}/2$ are satisfied. For $\gamma_{\mathrm{m}} n_{\mathrm{th}} < \kappa$, the NMS cooling mechanism can achieve ground state cooling but cannot realize to surpass the classical cooling limit within the range of $g_1\sqrt{\kappa/\gamma} > G > g_1\sqrt{\gamma_{\mathrm{m}} n_{\mathrm{th}}/\gamma}$. Therefore, for $\gamma_{\mathrm{m}} n_{\mathrm{th}} < \kappa$, the classical sideband cooling mechanism is more suitable for the ground state cooling.

In Fig. 8, it is given the time evolution of the phonon number for the cases of the classical sideband cooling ($g_1 = 0$), EIA, and NMS. In the EIA and NMS cases, the mechanical resonator can be cooled into its ground state, i.e., $n < 1$. With the same G, the time required for the ground state cooling in the EIA case is shorter than that of the NMS case and meanwhile the EIA case can achieve a smaller phonon number. In other word, the cooling effect of the EIA case is better than that of the NMS case with the same qubit dissipation rate γ. In the case of the classical sideband cooling ($g_1 = 0$), the ground state cooling is failed no matter in the strong ($G > \kappa$) or weak ($G < \kappa$) optomechanical coupling regime. For the classical sideband cooling, due to the influence of the classical cooling limit ($\gamma_{\mathrm{m}} n_{\mathrm{th}}/\kappa \approx 1$) in the strong optomechanical regime, a lower pre-cooling temperature (achieved $n_{\mathrm{th}} < 1000$) is required for cooling the mechanical resonator to its ground state. However, the classical cooling limit can be surpassed by the EIA-like or NMS cooling mechanism and make the ground state cooling possible under the strong optomechanical coupling. Obviously, the EIA-like cooling mechanism significantly enhances the cooling rate and surpassing the classical cooling limit compared to the classical resolved sideband cooling mechanism, so that result in reducing the requirement for low-temperature environments during ground-state cooling process. On the other hand, in high-Q cavities, the EIA-like cooling mechanism offers a higher cooling rate and can achieve better cooling outcomes compared to the EIT-like cooling mechanism. The EIT-like cooling mechanism is more suitable for unresolved sideband situations, where it can suppress the heating rate and overcome the limiting of resolved sideband condition.[36] Additionally, our scheme has several differences comparing with the previous work reported by Ref. [32]. First, this EIA-like ground state cooling is based on such a system where is composed of a higher-frequency mechanical resonator and two-level quantum systems with high dissipation rates; while the system is composed of a lower-frequency mechanical resonator and cold atoms with ultranarrow linewidths in Ref. [32]. Second, our scheme works on a small cavity detuning and the resolved sideband condition, while the scheme works on a large cavity detuning and the unresolved sideband condition in Ref. [32]. Third, this EIA-like cooling mechanism is based on the coupling between the new modes and mechanical resonator, and it overcome the classical cooling limit. However, the asymmetric Fano or EIT cooling mechanism[32] is based on the effective coupling between the atoms and mechanical resonator, and it overcome the limiting of the resolved sideband condition.

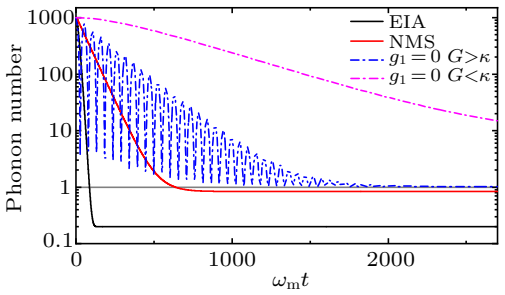


Fig. 8. Time evolution of the phonon number for different cases: the EIA case with $g_1 = 0.25\omega_{\mathrm{m}}$ and $\Delta_1 = \omega_{\mathrm{m}}$ (black solid line), the NMS case with $g_1 = 2\omega_{\mathrm{m}}$ and $\Delta_1 = -\omega_{\mathrm{m}}$ (red solid line), the strong optomechanical coupling regime with $g_1 = 0$ (bule dash-dotted line), and the weak optomechanical coupling ($G = 0.002\omega_{\mathrm{m}}$) case with $g_1 = 0$ (purple dash-dotted line). Other parameters are $\kappa = 0.01\omega_{\mathrm{m}}$, $\gamma = 1.02\omega_{\mathrm{m}}$, $G = 0.06\omega_{\mathrm{m}}$, $\gamma_{\mathrm{m}} = 10^{-5}\omega_{\mathrm{m}}$, and $n_{\mathrm{th}} = 1000$.

In experiments, such a two-level quantum system coupled to an optomechanical cavity can be realized by coupling atoms or nitrogen–vacancy (NV) centers to high-Q whispering-gallery-mode (WGM) cavities.[54,55] We take a set of experimentally feasible parameters as follows:[56–58] $\omega_{\mathrm{m}} = 2\pi \times 78$ MHz, $\kappa = 2\pi \times 6$ MHz, $g = 2\pi \times 3.4$ kHz, $\gamma_{\mathrm{m}} = 2\pi \times 4$ kHz, and $\gamma = 2\pi \times 63$ MHz. At this time, the qubit–cavity coupling strength can be set to $g_1 = 2\pi \times 17$ MHz ($0.22\omega_{\mathrm{m}}$) for satisfying $g_1 < (\kappa + \gamma)/4$ that is the condition for realizing the EIA-like cooling mechanism. For the

NMS cases, the qubit–cavity coupling strength can be set to $g_1 = 2\pi \times 78$ MHz $(1\omega_{\rm m})$ for satisfying $g_1 > (\kappa+\gamma)/4$, where g_1 can be controlled the number of qubits.[59] The thermal phonon number $n_{\rm th} = 1.686 \times 10^3$ at the temperature of $T = 1$ K in a ^{3}He cryostat. In order to cool the mechanical resonator to its ground state, the optomechanical coupling strength should be greater than $g_1\sqrt{\gamma_{\rm m} n_{\rm th}/\gamma} \approx 2\pi \times 5.56$ MHz and $\sqrt{\gamma_{\rm m} n_{\rm th}\gamma}/2 \approx 2\pi \times 10.31$ MHz for the EIA and NMS cases, indicating that the corresponding of intracavity photon number should be greater than 2.67×10^6 and 9.20×10^6, respectively. However, it is challenging to directly obtain the energy level structures of atoms or NV centers that satisfies the two-photon resonance condition with the cavity, while this may be solved by using a magnetic field to adjust energy level structures based on the Zeeman effect.[60,61] Moreover, the EIA cooling scheme can be extended by using an auxiliary cavity with a high dissipation rate to couple with the high-Q cavity. Experimentally, it is easier to achieve coupling between double WGM cavities, and by doping ions during the preparation of WGM cavities, the dissipation rates of both cavities can be altered while maintaining consistent eigen frequencies of both cavities[62] that has potential in realizing the EIA-like cooling scheme.

4. Conclusion and perspectives

In summary, we investigated a ground state cooling scheme by introducing the two-level quantum systems into a high-Q optomechanical cavity. Based on the perturbation theory, we derived the cooling rate, heating rate, and final phonon number using the noise approach. In the weak qubit–cavity coupling regime, we demonstrated the transition between EIT- and EIA-like effects through the noise spectra of the optical force, and the cooling rate is significantly enhanced by the EIA-like cooling mechanism under the optimal cooling condition. Furthermore, based on the dressed-state theory, we revealed that this EIA-like effect is formed by the quantum opposite destructive interference, which differs from the EIA effect caused by the quantum constructive interference in four-level atomic systems. In the strong qubit–cavity coupling regime, the system exhibits NMS of the optical field, achieving the optimal cooling rate at the red sideband relative to the splitting modes. The numerical results obtained by the covariance matrix method validate the reasonableness of the analytical results when the optomechanical coupling is much smaller than the qubit–cavity coupling. We also demonstrated that the final phonon number can exceed the classical cooling limit through the EIA-like cooling mechanism or the NMS cooling mechanism in the strong optomechanical coupling regime. Besides, the EIA-like ground state cooling can achieve a higher cooling rate and better cooling performance compared to the NMS case with the same qubit dissipation rate.

Acknowledgements

Project supported by the National Natural Science Foundation of China (Grant No. 11832016), the National Key Research and Development Program of China (Grant No. 2021YFB4000802), and the Steady Support Fund for the State Key Laboratory (Grant No. JBS242800180).

References

[1] Aspelmeyer M, Kippenberg T J and Marquardt F 2014 *Rev. Mod. Phys.* **86** 1391
[2] Barzanjeh S, Xuereb A, Gröblacher S, Paternostro M, Regal C A and Weig E M 2022 *Nat. Phys.* **18** 15
[3] Zhang Y, Hines A, Wilson D J and Guzman F 2023 *Phys. Rev. Appl.* **19** 054004
[4] Mahdavi V, Saghafifar H and Davoudi-Darareh M 2024 *Appl. Phys. B* **130** 99
[5] Zhang S D, Wang J, Zhang Q, Jiao Y F, Zuo Y L, Özdemir Ş K, Qiu C W, Nori F and Jing H 2024 *Opt. Quantum* **2** 222
[6] Dong C, Wang Y and Wang H 2015 *Natl. Sci. Rev.* **2** 510
[7] Bienfait A, Satzinger K J, Zhong Y P, Chang H S, Chou M H, Conner C R, Dumur É, Grebel J, Peairs G A, Povey R G and Cleland A N 2019 *Science* **364** 368
[8] Fiaschi N, Hensen B, Wallucks A, Benevides R, Li J, Alegre T P M and Gröblacher S 2021 *Nat. Photon.* **15** 817
[9] Bin Q, Jing H, Wu Y, Nori F and Lü X Y 2024 *Phys. Rev. Lett.* **133** 043601
[10] Sekatski P, Aspelmeyer M and Sangouard N 2014 *Phys. Rev. Lett.* **112** 080502
[11] Hauer B D, Combes J and Teufel J D 2023 *Phys. Rev. Lett.* **130** 213604
[12] Tobar G, Manikandan S K, Beitel T and Pikovski I 2024 *Nat. Commun.* **15** 7229
[13] Liu Y C, Hu Y W, Wong C W and Xiao Y F 2013 *Chin. Phys. B* **22** 114213
[14] Metcalfe M 2014 *Appl. Phys. Rev.* **1** 031105
[15] O'Connell A D, Hofheinz M, Ansmann M, Bialczak R C, Lenander M, Lucero E, Neeley M, Sank D, Wang H, Weides M, Wenner J, Martinis J M and Cleland A N 2010 *Nature* **464** 697
[16] Mancini S, Vitali D and Tombesi P 1998 *Phys. Rev. Lett.* **80** 688
[17] Metzger C H and Karrai K 2004 *Nature* **432** 1002
[18] Poggio M, Degen C L, Mamin H J and Rugar D 2007 *Phys. Rev. Lett.* **99** 017201
[19] Wilson-Rae I, Nooshi N, Zwerger W and Kippenberg T J 2007 *Phys. Rev. Lett.* **99** 093901
[20] Marquardt F, Chen J P, Clerk A A and Girvin S M 2007 *Phys. Rev. Lett.* **99** 093902
[21] Chan J, Alegre T P M, Safavi-Naeini A H, Hill J T, Krause A, Gröblacher S, Aspelmeyer M and Painter O 2011 *Nature* **478** 89
[22] Rivière R, Deléglise S, Weis S, Gavartin E, Arcizet O, Schliesser A and Kippenberg T J 2011 *Phys. Rev. A* **83** 063835
[23] Clark J B, Lecocq F, Simmonds R W, Aumentado J and Teufel J D 2017 *Nature* **541** 191
[24] Conteduca D, Reardon C, Scullion M G, Dell'Olio F, Armenise M N, Krauss T F and Ciminelli C 2017 *APL Photon.* **2** 086101
[25] Fu Z and Yang L 2022 *Phys. Rev. A* **105** L061504
[26] Sillanpää M A, Park J I and Simmonds R W 2007 *Nature* **449** 438
[27] Jiang X, Shao L, Zhang S X, Yi X, Wiersig J, Wang L, Gong Q, Lončar M, Yang L and Xiao Y F 2017 *Science* **358** 344
[28] Seri A, Corrielli G, Lago-Rivera D, Lenhard A, de Riedmatten H, Osellame R and Mazzera M 2018 *Optica* **5** 934
[29] Dobrindt J M, Wilson-Rae I and Kippenberg T J 2008 *Phys. Rev. Lett.* **101** 263602
[30] Liu Y C, Xiao Y F, Luan X and Wong C W 2013 *Phys. Rev. Lett.* **110** 153606

[31] Liu Y C, Shen Y F, Gong Q and Xiao Y F 2014 *Phys. Rev. A* **89** 053821
[32] Chen X, Liu Y C, Peng P, Zhi Y and Xiao Y F 2015 *Phys. Rev. A* **92** 033841
[33] Zhou B and Li G 2016 *Phys. Rev. A* **94** 033809
[34] Liu N, Chang R, Zhang S and Liang J Q 2022 *Int. J. Theor. Phys.* **61** 120
[35] Li T, Zhang S, Huang H L, Li F G, Fu X Q, Wang X and Bao W S 2018 *J. Phys. B: At. Mol. Opt. Phys.* **51** 045503
[36] Guo Y, Li K, Nie W and Li Y 2014 *Phys. Rev. A* **90** 053841
[37] Liu Y C, Xiao Y F, Luan X, Gong Q and Wong C W 2015 *Phys. Rev. A* **91** 033818
[38] Wang J 2021 *Chin. Phys. B* **30** 024204
[39] Fleischhauer M, Imamoglu A and Marangos J P 2005 *Rev. Mod. Phys.* **77** 633
[40] Taichenachev A V., Tumaikin A M and Yudin V I 1999 *Phys. Rev. A* **61** 011802
[41] Fu G, Li X, Zhuang Z, Zhang L, Yang L, Li X, Han L, Manson N B and Wei C 2008 *Phys. Lett. A* **372** 176
[42] Zhou Y L, Yan D and Li W 2022 *Phys. Rev. A* **105** 053714
[43] Braunstein D and Shuker R 2001 *Phys. Rev. A* **64** 053812
[44] Holstein T and Primakoff H 1940 *Phys. Rev.* **58** 1098
[45] Genes C, Vitali D and Tombesi P 2008 *Phys. Rev. A* **77** 050307
[46] Wu H, Li Y, Yang Z B and Zheng S B 2017 *Phys. Rev. A* **95** 013842
[47] Nie W, Chen A and Lan Y 2015 *Opt. Express* **23** 30970
[48] Sarma B and Sarma A K 2016 *Phys. Rev. A* **93** 033845
[49] Zhang X Y, Zhou Y H, Guo Y Q and Yi X X 2018 *Phys. Rev. A* **98** 033832
[50] Mirza I M, Ge W and Jing H 2019 *Opt. Express* **27** 25515
[51] Liao K Y, Tu H T, Yang S Z, Chen C J, Liu X H, Liang J, Zhang X D, Yan H and Zhu S L 2020 *Phys. Rev. A* **101** 053432
[52] Sun Y, Yang Y, Chen H and Zhu S 2015 *Sci. Rep.* **5** 16370
[53] Tassin P, Zhang L, Zhao R, Jain A, Koschny T and Soukoulis C M 2012 *Phys. Rev. Lett.* **109** 187401
[54] Aoki T, Dayan B, Wilcut E, Bowen W P, Parkins A S, Kippenberg T J, Vahala K J and Kimble H J 2006 *Nature* **443** 671
[55] Barclay P E, Santori C, Fu K M, Beausoleil R G and Painter O 2009 *Opt. Express* **17** 8081
[56] Verhagen E, Deléglise S, Weis S, Schliesser A and Kippenberg T J 2012 *Nature* **482** 63
[57] Poggiali F, Cappellaro P and Fabbri N 2017 *Phys. Rev. B* **95** 195308
[58] Panadero I, Espinós H, Tsunaki L, Volkova K, Tobalina A, Casanova J, Acedo P, Naydenov B, Puebla R and Torrontegui E 2024 *Phys. Rev. Appl* **22** 014035
[59] Liu T, Zhao J L, Guo B Q, Wu Q C, Zhou Y H and Yang C P 2021 *Phys. Rev. A* **103** 023706
[60] Kellerbauer A, Fischer A and Warring U 2014 *Phys. Rev. A* **89** 043430
[61] Li B, Li P B, Zhou Y, Ma S L and Li F L 2017 *Phys. Rev. A* **96** 032342
[62] Peng B, Özdemir Ş K, Lei F, Monifi F, Gianfreda M, Long G L, Fan S, Nori F, Bender C M and Yang L 2014 *Nat. Phys.* **10** 394